Nano Energy 65 (2019) 104053

Contents lists available at ScienceDirect

Nano Energy

journal homepage: www.elsevier.com/locate/nanoen

Communication

Boosting the photocatalytic hydrogen evolution performance via an atomically thin 2D heterojunction visualized by scanning photoelectrochemical microscopy

Jae Yoon Lee[a], Sungwoo Kang[b], Donghun Lee[a], Seokhoon Choi[b], Seunghoon Yang[a], Kangwon Kim[c], Yoon Seok Kim[a], Ki Chang Kwon[b], Soo ho Choi[d], Soo Min Kim[e], Jihoon Kim[f], Jungwon Park[f,g], Haeli Park[a], Woong Huh[a], Hee Seong Kang[a], Seong Won Lee[h], Hong-Gyu Park[a,h], Min Jae Ko[i], Hyeonsik Cheng[c], Seungwu Han[b,**], Ho Won Jang[b,**], Chul-Ho Lee[a,*]

[a] KU-KIST Graduate School of Converging Science and Technology, Korea University, Seoul, 02841, Republic of Korea
[b] Department of Materials Science and Engineering, Research Institute of Advanced Materials, Seoul National University, Seoul, 08826, Republic of Korea
[c] Department of Physics, Sogang University, Seoul, 04107, Republic of Korea
[d] Department of Physics, Dongguk University, Seoul, 04620, Republic of Korea
[e] Korea Institute of Advanced Composite Materials, Korea Institute of Science and Technology (KIST), Wanju-Gun, 55324, Republic of Korea
[f] Department of Chemical and Biological Engineering, Seoul National University, Seoul, 08826, Republic of Korea
[g] Center for Nanoparticle Research, Institute for Basic Science (IBS), Seoul, 08826, Republic of Korea
[h] Department of Physics, Korea University, Seoul, 02841, Republic of Korea
[i] Department of Chemical Engineering, Hanyang University, Seoul, 04763, Republic of Korea

ARTICLE INFO

Keywords:
Photoelectrochemical hydrogen evolution
Transition metal dichalcogenides
Heterojunction
Catalyst
Spatially resolved PEC characterization

ABSTRACT

Heterojunction catalyst can facilitate efficient photoelectrochemical (PEC) hydrogen evolution by reducing a potential barrier for charge transfer at the semiconductor/electrolyte interface. Such a heterojunction effect at the atomic thickness limit has not yet been explored although it can be strengthened because of strong built-in field and ultrafast charge transfer across the junction. Here, we first investigate a novel strategy to boost the hydrogen evolution performance of the *p*-type WSe_2 photocathode via reducing the overpotential with an atomically thin heterojunction catalyst comprising MoS_2 and WS_2 monolayers. To unveil an effective role of the heterojunction by isolating its kinetic contribution from other collective catalytic effects, we develop and utilize an *in situ* scanning PEC microscopy, which enables the spatially-resolved visualization of the enhanced photocatalytic hydrogen evolution performance of the heterojunction. Notably, significant reduction in overpotential, from $+0.28 \pm 0.03$ to -0.04 ± 0.05 V versus (vs.) the reversible hydrogen electrode (RHE), is achieved when the MoS_2/WS_2 heterojunction is introduced as a catalyst even without intentional generation of catalytic sites. As a result, the photocurrent of $\sim 4.0\ mA\ cm^{-2}$ occurs even at 0 V vs. RHE. Furthermore, the beneficial effect of the atomically scaled vertical heterojunction is explained by the built-in potential resulted from efficient charge transfer in type-II heterojunctions with the support of first-principles calculations. Our demonstration not only offers an unprecedented approach to investigating the fundamental PEC characteristics in relation to the tailored properties of a catalyst but also proposes a new catalytic architecture, thereby enabling the design of highly efficient PEC systems.

1. Introduction

The demand for new catalytic materials and/or architectures toward realizing efficient photoelectrochemical (PEC) hydrogen generation is insatiable [1–8]. Recently, two-dimensional (2D) layered transition metal dichalcogenides (TMDs) such as MoS_2 have emerged as promising candidates for nonprecious and earth-abundant catalysts [2–4,9–19]. In particular, the atomic edges of the layered structure have been identified as a thermodynamically active site, and thus considerable research efforts have been devoted to maximizing such catalytic sites for efficient hydrogen

* Corresponding author.
** Corresponding authors.
E-mail addresses: hansw@snu.ac.kr (S. Han), hwjang@snu.ac.kr (H.W. Jang), chlee80@korea.ac.kr (C.-H. Lee).

https://doi.org/10.1016/j.nanoen.2019.104053
Received 25 June 2019; Received in revised form 30 July 2019; Accepted 26 August 2019
Available online 30 August 2019
2211-2855/ © 2019 Elsevier Ltd. All rights reserved.

evolution reaction (HER) [11–14,18–23]. To fully exploit large surface-to-edge ratio of 2D materials, additionally, the inert basal planes of those layered structures have been activated via creating atomic vacancies or incorporating catalytic dopants [24,25]. Particularly for solar-driven photoelectrode applications, using surface-activated atomically thin planar catalysts can be desirable because it offers synergetic advantages in concurrently achieving high light absorption and effective surface passivation of underlying photoactive semiconductors as well as fully utilizing large active area [16,22].

In addition to the optimization of thermodynamically active sites, to further improve the PEC performance, the photoexcited charges must be efficiently separated and transferred from the solid-state photocathode to the liquid-phase electrolyte. In pursuit of this goal, many previous studies have attempted to utilize heterojunctions that form a staggered alignment between the conduction band edge of a *p*-type semiconductor and the hydrogen reduction potential ($-qE^{\circ}$ (H^{+}/H_2)) [5,6], promoting electron transfer at the interface. In this respect, the ability to build band-engineered heterostructures using various TMDs with different band alignments and ultrafast charge transfer in those atomically thin heterojunctions can offer unexplored opportunities to optimize the interfacial kinetics of photoelectrolysis [26–29]. Nevertheless, such exceptional capability of TMD heterojunctions have rarely been employed to boost charge transfer at the semiconductor/electrolyte interface, and their roles in HER have not yet been revealed due to experimental challenges in excluding various catalytic effects during typical PEC measurements.

Here, we first explore the possibility of utilizing an atomically thin TMD heterojunction as a catalyst to reduce the overpotential for the HER on a *p*-type semiconductor photocathode. The enhanced HER performance by the heterojunction catalyst is successfully visualized by using spatially resolved *in situ* PEC characterization platform. The newly developed methodology allows us to characterize the photocatalytic HER performance of the atomically thin heterojunction while excluding the collective effects of various active sites that may exist in these layered materials.

2. Results and discussion

Fig. 1a shows the schematic band diagram of a model system used in this study, illustrating that an atomically thin heterojunction catalyst can reduce the overpotential for the HER. The system consists of a monolayer MoS_2/WS_2 heterojunction as the catalyst and underlying ~80 nm-thick WSe_2 layers with a bottom graphene electrode as the photocathode. The MoS_2/WS_2 heterojunction on the *p*-type WSe_2 layer is theoretically predicted to form a cascade band alignment. The edge positions of conduction band minimum and valence band maximum of

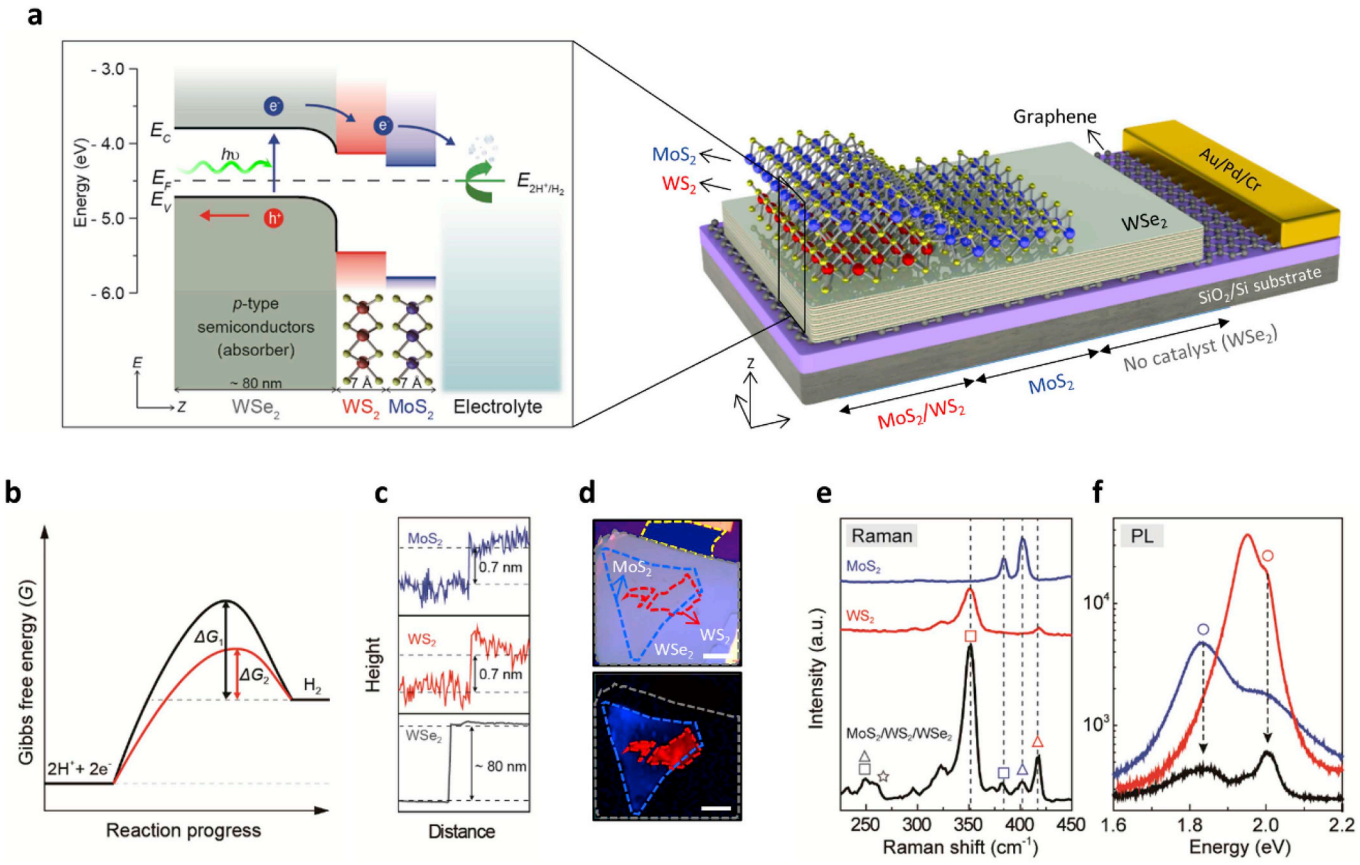

Fig. 1. Atomically thin heterojunction catalyst for HER on a *p*-type semiconducting photocathode. (a) Band diagram (left) and schematic (right) of a photocathode with the monolayer MoS_2/WS_2 heterojunction as a catalyst and underlying ~80 nm-thick WSe_2 layers with a bottom graphene electrode. The staggered type-II band alignment can promote the separation and transport of photoexcited electrons from the light-absorbing WSe_2 layer to the electrolyte. (b) General changes in Gibbs free energy according to the reaction progress with (red solid line, ΔG_2) or without (black solid line, ΔG_1) the monolayer MoS_2/WS_2 heterojunction catalyst. (c) Line profiles of height of monolayer MoS_2 (top), monolayer WS_2 (middle), and ~80 nm-thick WSe_2 (bottom). (d) Optical image (top) and merged PL mapping image (bottom) of the fabricated heterostructure. Red, blue, gray, and yellow dashed lines indicate the boundaries of WS_2, MoS_2, WSe_2, and graphene, respectively. In the PL map, red and blue correspond to the direct bandgap transition at 2.00 eV for WS_2 and 1.85 eV for MoS_2, respectively. Scale bars are 10 μm. (e) Raman spectra of the $MoS_2/WS_2/WSe_2$ heterostructure (black solid line), monolayer MoS_2 (blue dashed line), monolayer WS_2 (red dashed line) and ~80 nm-thick WSe_2 (gray dashed line) (left). Squares, triangles, and a star in gray (WSe_2), red (WS_2), and blue (MoS_2) represent the E^1_{2g}, A_{1g}, and 2LA(M) modes respectively. (f) PL spectra of the $MoS_2/WS_2/WSe_2$ heterostructure (black solid line), monolayer MoS_2 (blue dashed line), and monolayer WS_2 (red dashed line) (right). Blue and red circles represent the direct bandgap transition at 1.85 and 2.00 eV for MoS_2 and WS_2, respectively. (For interpretation of the references to color in this figure legend, the reader is referred to the Web version of this article.)

TMDs are drawn using theoretically calculated values in the previous literature [26]. The resultant type-II band alignment can facilitate the separation and transport of photoexcited charges from the light-absorbing WSe_2 layer to the electrolyte. Importantly, because both the MoS_2 and WS_2 layers are atomically thin, the depletion region is distributed throughout the entire junction with a thickness of ~1.4 nm, generating a substantial built-in potential [27,28]. The resulting electric field at the electrolyte/photocathode interface is expected to significantly improve the efficiency of the HER by reducing the potential barrier (ΔG) required for hydrogen reduction reaction [$2H^+ + 2e^- \rightarrow H_2$] (Fig. 1b). Note that such interfacial engineering at the atomic thickness limit is possible due to the formation of pinning-free van der Waals (vdW) interfaces between layered TMD materials [30]. However, the use of photoactive materials is not restricted to semiconducting TMDs as long as it forms the appropriate band alignment.

We fabricated the designed model system composed of $MoS_2/WS_2/WSe_2$/graphene heterostructures using mechanical transfer and sequential vdW stacking of exfoliated or chemical vapor-deposited constituent layers (see the details of the device fabrication procedure in section S1) [31,32]. Before the mechanical transfer, the thickness of monolayer MoS_2, monolayer WS_2 and the thick WSe_2 layer were confirmed by atomic force microscopy (Figs. 1c and S3). As shown in the optical image in Fig. 1d, the fabricated heterostructure contains three spatially distinct regions, namely, $MoS_2/WS_2/WSe_2$, MoS_2/WSe_2, and WSe_2, which allows us to investigate the catalytic effects of differently stacked heterostructures on the HER without experimental sample-to-sample variations in the subsequent PEC measurements.

The vertically stacked heterostructure is characterized by Raman and photoluminescence (PL) spectroscopy. All the spectral features of 383.04 (E^1_{2g}) and 401.64 (A_{1g}) cm^{-1} of monolayer MoS_2 (the frequency differences of 18.64 cm^{-1}), 351.92 (E^1_{2g}) and 417.14 (A_{1g}) cm^{-1} of monolayer WS_2 (the frequency differences of 66.23 cm^{-1}), and 249.39 (E^1_{2g} and A_{1g}) cm^{-1} and 259.92 (2LA(M)) cm^{-1} of bulk WSe_2, were clearly observed (Fig. 1e), confirming the formation of the $MoS_2/WS_2/WSe_2$ heterostructure [33,34]. In addition, in the PL spectra of Fig. 1f, the direct bandgap emissions from individual monolayer MoS_2 (1.85 eV) and monolayer WS_2 (2.00 eV) are clearly visible, as shown in the PL mapping image in Fig. 1d, but strongly quenched at the stacked area by an order of magnitude in their intensities. This indicates that ultrafast charge transfer spontaneously occurs as a result of the cascade

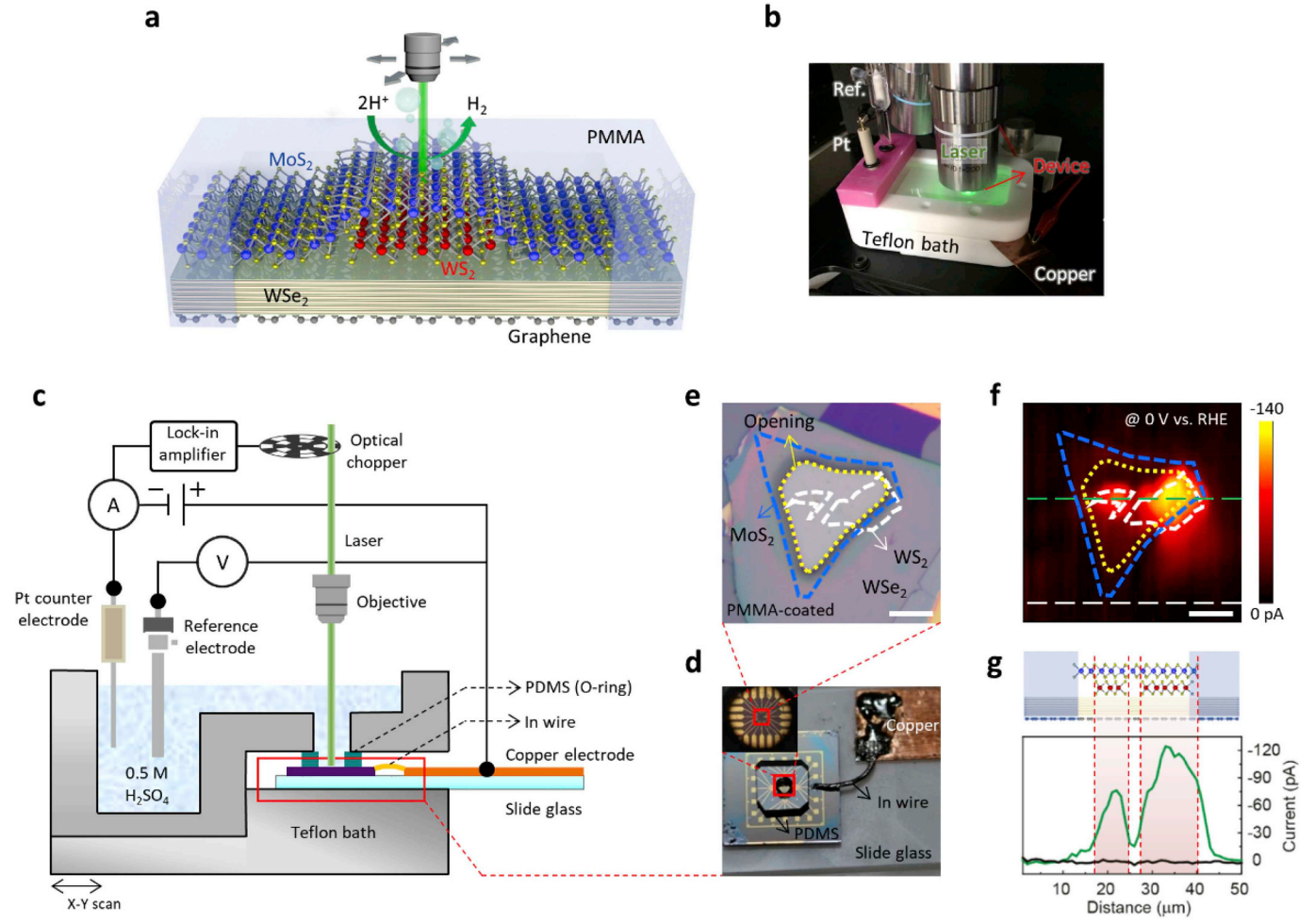

Fig. 2. Spatially resolved PEC characterization for visualizing photocatalytic activities. (a) Schematic illustration and (b) Photograph of the measurement with a 532 nm laser and a mapping stage. (c) Schematic of the SPECM measurement set-up, combining scanning photocurrent microscopy with a standard three-electrode electrochemical measurement. A copper electrode contacting the device, Pt, and the saturated calomel electrode are used as the working, counter, and reference electrodes, respectively. The home-designed reaction bath is illuminated by a 532 nm laser from above. (d) Photograph of the PMMA-passivated device on the SiO_2/Si substrate covered with the PDMS (O-ring). The device is electrically connected to a copper electrode through an In wire. (e) Optical image of the microfabricated device with lithographic opening. (f) Photocurrent mapping image of the device at 0 V vs. RHE. In (e) and (f), the blue dashed line, the white dashed line, and the yellow dotted line indicate the boundaries of MoS_2, WS_2, and the lithographic opening area, respectively. Scale bars in (e) and (f) are 10 μm. (g) Schematic side view of the device along the green dashed line in (f) (top) and corresponding line profiles of photocurrent along the dashed lines in (f) (bottom). Green and black line profiles are obtained along the green and white dashed lines in (f), respectively. Red shaded regions between red dashed lines indicate the MoS_2/WS_2 heterojunctions. (For interpretation of the references to color in this figure legend, the reader is referred to the Web version of this article.)

band alignment formed in the $MoS_2/WS_2/WSe_2$ heterojunctions as theoretically predicted (inset of Fig. 1a), which is also consistent with previous experimental results in this type of heterostructure with the staggered band alignment [27–29]. The charge transfer and interaction between the layers are further investigated by using scanning Kevin probe microscopy (SKPM) and X-ray photoelectron spectroscopy (XPS) (see the details of results and discussions in the section S5 and S7). It is also worth noting that the incident light is mostly absorbed by the underlying WSe_2 photocathode while absorption by the top catalyst consisting of MoS_2 and WS_2 monolayers is relatively negligible (see the reflection spectra in Fig. S5).

To carefully prove our hypothesis that an atomically thin heterojunction catalyst can reduce the overpotential for the HER, we first developed a spatially resolved PEC characterization platform employing an *in situ* microscopic photocurrent mapping technique combined with standard three-electrode electrochemical measurements in a home-designed reaction bath (Fig. 2a and b). In the case of commonly used PEC measurements with large-area photoelectrodes under global illumination, the exact correlation of PEC performance with the specific properties of the heterostructures and study of the corresponding HER mechanism are difficult due to the ensemble averaging effects of various active sites such as step edges, vacancies, and grain boundaries, as well as other extrinsic factors including contact resistances, the number of layers, and local strains [11,12,23,25,35–41]. To address such an issue, we used a specialized set up for scanning photoelectrochemical microscopy (SPECM) measurements as schematically described in Fig. 2c. For the microscale PEC measurements, the active area directly exposed to the electrolyte solution could be defined roughly by an elastomeric O-ring and constricted specifically by lithographic patterning of the microfabricated device (photographs in Fig. 2d and e). Then, while the focused laser scans over the exposed area using either a motorized microstage or a scanning mirror, the photocurrent generation is measured and mapped according to the position of the laser spot. The focused spot size is less than ~1.0 μm in diameter and the incident power is as low as ~100 nW to exclude photothermal effects caused by local heating [42]. This analysis enables the spatially resolved PEC imaging and visualization of the photocatalytic activities on different catalytic surfaces.

To clearly reveal the effects of the TMD heterojunction on the HER compared to those of the single TMD layer, as shown in Fig. 2e, we fabricated the device with a lithographic opening that contains only the MoS_2 and MoS_2/WS_2 regions. The patterned area exposes the same

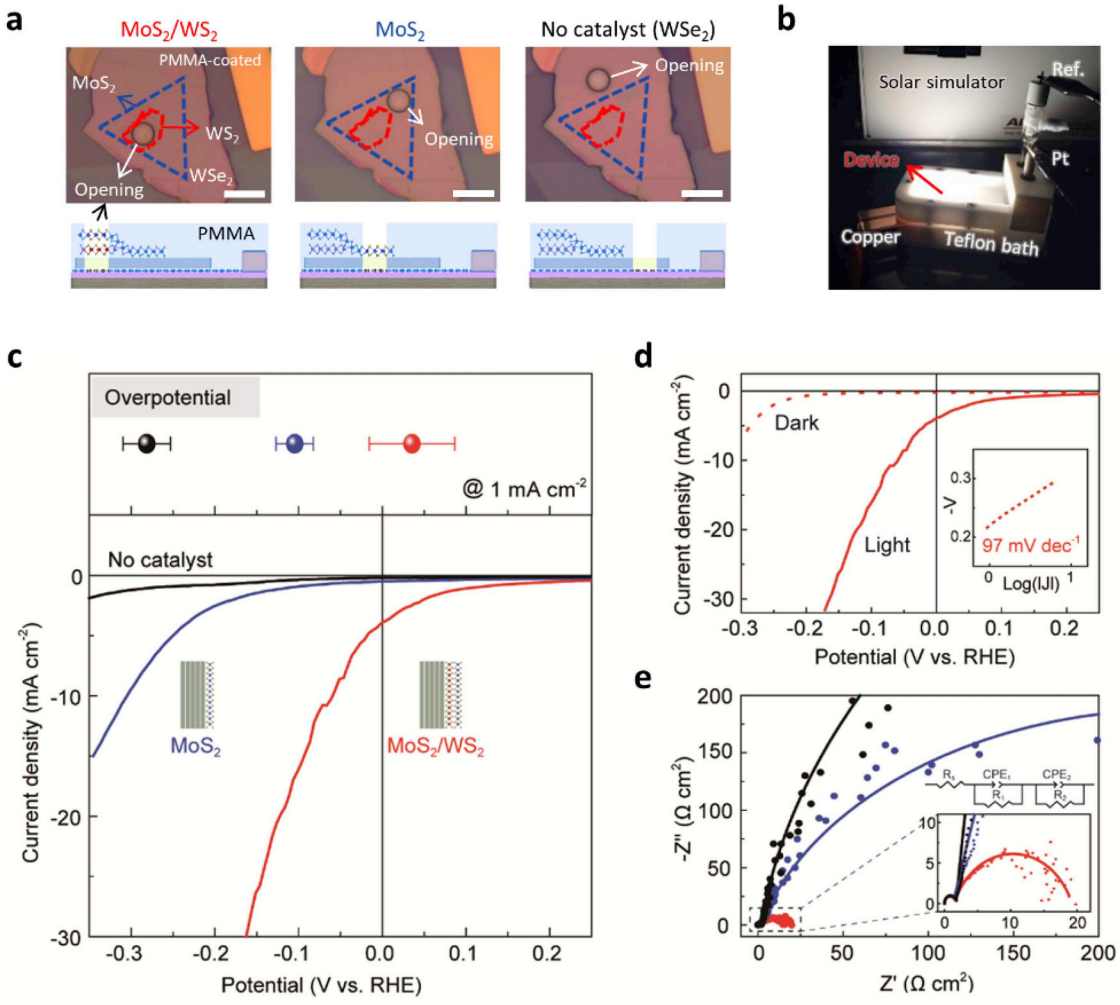

Fig. 3. Spatially defined PEC characterization on different catalytic surfaces under global illumination. (a) Optical images and schematic side views of the devices with circular opening patterns (radius = 2 μm) corresponding to $MoS_2/WS_2/WSe_2$ (left), MoS_2/WSe_2 (middle) and no catalyst (bare WSe_2, right) areas. Scale bars are 10 μm. (b) Photograph of the measurement under global illumination with a solar simulator. (c) Polarization curves (bottom panel) and statistics of the overpotential (top panel) of each structure. (d) Polarization curves of the $MoS_2/WS_2/WSe_2$ heterostructure measured in the dark (red dashed line) and under 1 Sun illumination (red solid line). Inset: Tafel slope in the dark plotted as log (J) against potential vs. RHE. (e) Nyquist impedance plots of each structure under illumination at −0.14 V vs. RHE from 350 kHz to 0.1 Hz. The semicircular traces represent the fitting curves using the inset equivalent circuit including the charge-transfer resistance (R_1) across the graphene/TMDs heterostructures and charge-transfer resistance (R_2) from the topmost TMD layer to the electrolyte. The inset is the magnified graph of the dashed box. (For interpretation of the references to color in this figure legend, the reader is referred to the Web version of this article.)

MoS_2 basal surface to the electrolyte solution while the poly (methyl methacrylate) (PMMA) layer passivates the edges of MoS_2 (or WS_2). This configuration enables direct comparison between the MoS_2/WS_2 heterojunction and the monolayer MoS_2, eliminating the catalytic effects of other active sites such as edges. Fig. 2f shows the photocurrent mapping image obtained at 0 V versus (vs.) the reversible hydrogen electrode (RHE). In the map, negligible photocurrent (< 1 pA) is measured from the PMMA-passivated area (the black colored line profile in Fig. 2g), and the differently stacked regions are clearly distinguished from the opened area. The photocurrent generated from the overlapped MoS_2/WS_2 area is approximately 10 times higher than that from the MoS_2 area. This result indicates that the HER is more strongly activated on the MoS_2/WS_2 than on the MoS_2 surface as we hypothesized. For this particular device, as presented in the photocurrent line profile of Fig. 2e (green colored line), two MoS_2/WS_2 regions that are ~2–3 μm apart are spatially resolved in the photocurrent map.

The spatial resolution achieved in our measurements is approximately a few micrometers although there is the slight drift in the mapping image presumably due to light scattering and stage drift during the scanning measurement inside the electrolyte solution. This value is even higher than that of scanning electrochemical microscopic measurements over the strained MoS_2 basal plane with sulfur vacancies [40] although it is slightly lower than those (~1 μm) from photocurrent mapping in typical solid-state devices. Nevertheless, it turned out that the developed SPECM can be universally exploited to characterize how the PEC performances are affected by other factors such as thickness of the heterojunction and presence of edges on the heterojunction (see additional PEC mapping results in Figs. S7 and S8). Although we focused on the atomically thin heterojunction in this work, it is worth noting that the heterojunction effect became worse when the few-layered WS_2 instead of the monolayer was used to form the heterojunction due to large charge-transfer resistances for layer-to-layer hoping and weak built-in field (see Fig. S7).

To clarify the enhanced HER at the heterojunction and obtain further quantitative analyses, we performed spatially defined PEC characterization with an almost identical platform except with a global illumination source instead of a focused scanning laser. For these measurements, we exposed only the specific area including the heterostructure of interest. Fig. 3a shows optical images and schematic side views of the microscale devices with different circular opening patterns (radius = 2 μm) corresponding to the $MoS_2/WS_2/WSe_2$, MoS_2/WSe_2, and WSe_2 areas. Using those devices, the HER performance was then measured under global illumination with a solar simulator (Fig. 3b), and the representative polarization curves of each structure were presented in Fig. 3c. Obviously, the onset potential shifts to lower values upon the introduction of the MoS_2 and MoS_2/WS_2 catalysts on the WSe_2 photocathode. The statistically obtained overpotentials at a photocurrent density of 1 mA cm^{-2} are +0.28 ± 0.03, +0.10 ± 0.02, and −0.04 ± 0.05 V vs. RHE for the no catalyst (bare WSe_2), MoS_2, and MoS_2/WS_2 surfaces, respectively (top panel of Fig. 3c). These results clearly indicate that the significant reduction in overpotential is achieved solely by the heterojunction without surface activation, and the value is even smaller than those of 2H-phase MoS_2 edges on the *p*-Si photocathode [22].

In addition, as shown in Fig. 3d, the WSe_2 photocathode with the MoS_2/WS_2 heterojunction catalyst exhibits a significant photoresponse with the reduced overpotential, and the photocurrent of 4.0 mA cm^{-2} thus occurs even at 0 V vs. RHE. The dark current is smaller than the photocurrent by more than an order of magnitude, and the Tafel slope is estimated to be ~97 mV dec^{-1}, as plotted in the inset of Fig. 3d. A value higher than 39 mV dec^{-1} suggests that the HER mechanism is still dominantly determined by Heyrovsky or Volmer reactions because the MoS_2 basal surface has not been intentionally activated by the generation of additional catalytic sites other than naturally existing sulfur vacancies [23,41]. The Tafel slope is very similar for the monolayer MoS_2, at ~110 mV dec^{-1}, but this value is approximately three times smaller than that of the bare WSe_2 surface (Fig. S10), implying that the hydrogen adsorption energy on the MoS_2 basal surface may not be significantly altered by the underlying WS_2 layer that forms the heterojunction. This is consistent with the previously reported first-

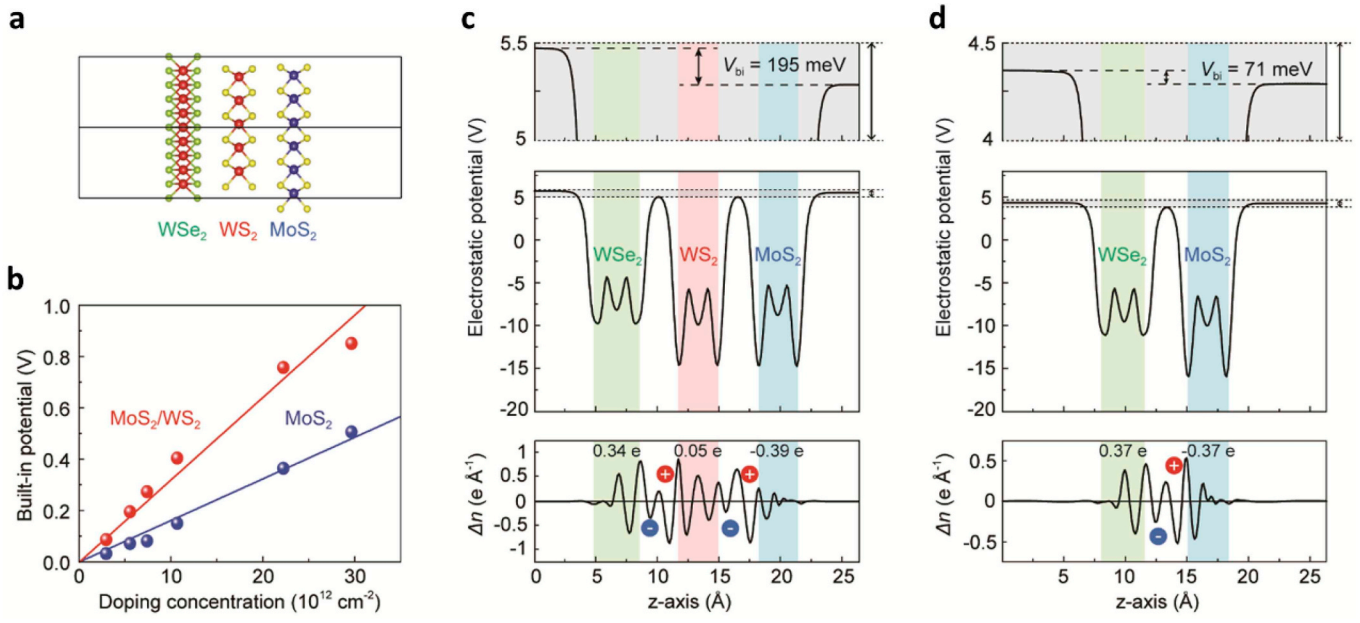

Fig. 4. DFT calculation. (a) A model system for the $MoS_2/WS_2/WSe_2$ heterostructure. (b) Built-in potential of the MoS_2 (blue circle) and the MoS_2/WS_2 heterojunction (red circle) the on *p*-type WSe_2 layer as a function of doping concentration, respectively. The solid lines represent the fitting lines. (c) and (d) The *x-y* plane-averaged electrostatic potential (middle panel), the enlarged potential in vacuum regions (top panel), and the *x-y* plane-averaged charge density difference (Δn) (bottom panel) of (c) the $MoS_2/WS_2/WSe_2$ heterojunction and (d) the MoS_2/WSe_2 heterojunction. The built-in potential (V_{bi}) values are indicated by arrows in the graphs. In the calculation, MoS_2 and WSe_2 are electron-doped and hole-doped semiconductors, respectively, with doping concentrations of 5.56×10^{12} cm^{-2}, and WS_2 is an intrinsic layer. The integral charge values in both structures are equal to zero. (For interpretation of the references to color in this figure legend, the reader is referred to the Web version of this article.)

principles calculations; the sulfur vacancy, the widely accepted active site on the basal plane of MoS_2, develops defect levels deep in the band gap [43]. Since the charge transfer from MoS_2 to the underlayers occurs with doped electrons close to the conduction band, the charge distribution at the sulfur vacancy would be largely unaffected, resulting in similar hydrogen adsorption energy regardless of the amount of charge transfer. This explanation also implies that the MoS_2/WS_2 heterojunction could lead to the electrostatic reduction of the overpotential at the electrolyte/photocathode interface without intentional generation of active sites on the MoS_2 surface.

This enhancement of the PEC performance can be further confirmed by electrochemical impedance spectroscopy (EIS) to measure the charge-transfer resistance at the interfaces. Fig. 3e presents the Nyquist plot of each structure, showing two components, the charge-transfer resistance (R_1) from the electrode to the semiconductor and the charge-transfer resistance (R_2) from the semiconductor to the electrolyte. Due to the atomically thin thickness of MoS_2 and WS_2, the charge-transfer resistances across the layers from WSe_2 to MoS_2 are negligible. For all three structures, R_1 values less than $2\,\Omega\,cm^2$, indicated by small semicircles in the plots, are very low because of the good electrical contact between the WSe_2 and the graphene. On the other hand, the R_2 value for the MoS_2/WS_2 ($18\,\Omega\,cm^2$) is considerably lower than those for the other structures (490 and $1{,}200\,\Omega\,cm^2$ for MoS_2 and WSe_2, respectively). This result strongly suggests the improvement of the HER kinetics in the atomically thin heterojunction, which is consistent with the observed reduction in the overpotential. Note that the enhanced PEC performances in terms of overpotential and charge-transfer resistance are repeatedly measured from our samples. The stability of the catalyst during a series of PEC measurements including SPECM is confirmed by comparing the Raman spectra before and after the measurement. Raman peaks of each constituent layer are preserved without noticeable peak shift and degradation (see Fig. S9).

To support the experimentally observed results, theoretical modeling was carried out using the first-principles calculations based on the density functional theory (DFT) (see the details of DFT calculation in section S12). We investigated the generation of the built-in potential (V_{bi}) as a result of charge transfer within the atomically thin TMD heterojunction, which eventually leads to reduced overpotential. Fig. 4a is a modeling system for the $MoS_2/WS_2/WSe_2$ heterostructure. In this model, MoS_2, WS_2, and WSe_2 are assumed to be electron-doped, undoped, and hole-doped, respectively, which may be reasonable according to previous literature [44]. Fig. 4b plots the calculated V_{bi} of the MoS_2 (blue circle) and the MoS_2/WS_2 heterojunction (red circle) on the WSe_2 layer as a function of doping concentration. Once the heterojunctions are formed, electrons transfer from MoS_2 to WSe_2, developing V_{bi} across the heterojunction. The V_{bi} increases linearly as the doping concentration increases, and the values for the MoS_2/WS_2 heterojunction are always larger than those of the MoS_2 regardless of doping. Especially at the concentration of $5.56 \times 10^{12}\,cm^{-2}$ for both *n*-type MoS_2 and *p*-type WSe_2, the electrostatic potential profiles of the MoS_2/WSe_2 and $MoS_2/WS_2/WSe_2$ heterojunctions are shown in Fig. 4c and d, respectively. The values of V_{bi} measured by the potential difference between the left and right vacuum level are 195 and 71 meV for $MoS_2/WS_2/WSe_2$ and MoS_2/WSe_2, respectively. The larger V_{bi} for $MoS_2/WS_2/WSe_2$ than for MoS_2/WSe_2 is consistent with the surface potential measured by SKPM (Fig. S4) and the observed reduction in the overpotential. The charge transfers from MoS_2 to WSe_2 can be evaluated by the plane-averaged electron density difference (see bottom panels of Fig. 4c and d) and are ca. 0.5e per dopant in both structures. Even though the amount of charge transfer is similar, V_{bi} is larger when WS_2 is inserted because of the increased distance between the positive and negative charges. That is, the charge-neutral WS_2 layer acts as a pure dielectric medium in the simple capacitor model. Since this enhancement of V_{bi} in the presence of a dielectric WS_2 layer is based on a general principle of electrostatics, it should effectively apply to any doping level.

3. Conclusion

In summary, we successfully demonstrated that an atomically thin heterojunction can be employed as an HER catalyst to reduce an overpotential through specialized PEC measurements that enable spatially resolved characterization on different catalytic surfaces or architectures. The built-in potential generated by the atomically thin TMD heterojunctions is dominantly responsible for significant reduction in both overpotential and charge-transfer resistance. This offers an unexplored strategy to improve photocatalytic activities by engineering the interfacial kinetics of charge transfer in addition to optimizing the thermodynamics of active sites. Our demonstration represents a model system that can be applied to the study and design of atomically thin catalysts for a variety of light-driven electrochemical processes, including solar-to-fuel conversion.

4. Experimental section

4.1. Device fabrication

Microscale devices composed of TMD and graphene layers, acting as a photocathode, were fabricated on the SiO_2/Si substrate with prepatterned electrodes using typical mechanical transfer and vdW stacking techniques. Monolayer MoS_2 grown by chemical vapor deposition (CVD) [32] and monolayer WS_2, few-layer WSe_2, and few-layer graphene exfoliated from single crystals were used as constituent layers. Few-layer graphene was employed in the device as a contact electrode to reduce the contact resistance. The electrical contact between the graphene and the prepatterned electrode is formed by *e*-beam lithography and metal evaporation (Au/Pd/Cr (40/15/3 nm)). Then, to expose the areas of interest for the subsequent PEC measurements, we performed additional *e*-beam lithography.

4.2. Material characterization

Raman and PL spectra were obtained using a home-built spectrometer equipped with a monochromator (Andor, SOLIS 303i) and an excitation laser of 532 nm. The signal was collected by an objective lens (NIKON 100 ×, N.A. = 0.9), and dispersed by 1,200 and 300 line mm^{-1} gratings for Raman and PL measurements, respectively. Atomic force microscopy (Park systems, XE-10) was performed to identify the surface morphology and thickness of each layer of the TMDs and graphene and to measure the surface potentials of the heterostructures with a conducting cantilever tip. Reflection measurements were performed at room temperature using broadband emission from a supercontinuum laser (Fianium, sc-400), in conjunction with a beam splitter and an objective (50 ×, N.A. = 0.8). XPS (ULVAC-PHI, X-tool) was performed with Al K_α X-ray source (1486.6 eV) under ultrahigh vacuum ($\sim 10^{-10}$ Torr).

4.3. Spatially resolved and spatially defined PEC measurements

All PEC measurements were performed by an Ivium potentiostat (Ivium Technologies, Compact-stat) with a three-electrode system using a Pt wire as a counter electrode, a saturated calomel reference electrode, and a working electrode in a 0.5 M H_2SO_4 standard electrolyte solution. The three-electrode system was built inside a home-designed reaction bath. For scanning photocurrent measurements, we used a 532 nm laser with a motorized microstage or Galvano mirrors. Photocurrent was measured at constant voltage (0 V vs. RHE) using a lock-in amplifier (Stanford Research Systems, SR830) with an optical chopping frequency of ~100 Hz. A Xe arc lamp calibrated to an output power of $100\,mW\,cm^{-2}$ (corresponding to the AM 1.5 G condition) was used as a global illumination source. A scan rate of $10\,mV\,s^{-1}$ was used for the linear sweep. EIS was conducted by applying a constant potential of −0.14 V vs. RHE with a sweeping frequency from 350 kHz to 0.1 Hz.

4.4. DFT calculation

The first-principles calculations were performed using Vienna *Ab initio* Simulation Package (VASP) [45]. The generalized gradient approximation was employed for the exchange-correlation functional [46] for electrons and the energy cutoff for the plane-wave basis set was 300 eV. The van der Waals interaction was included empirically [47]. A vacuum slab with a thickness of 18 Å was inserted, and the dipole correction was used to remove spurious interaction within the periodic boundary condition. Because of lattice mismatch, we used 11.4 × 11.4 and 16.4 × 16.4 $Å^2$ for undoped MoS_2/WSe_2 and $MoS_2/WS_2/WSe_2$ heterostructures, respectively, by applying a lattice strain of ~0.1%. To simulate the built-in potential as a function of doping concentration, we further expanded the lateral periodicity for MoS_2/WSe_2 and $MoS_2/WS_2/WSe_2$, and replaced Mo (W) atoms with Re (Nb) for electron (hole) doping. For *k*-point sampling, 3 × 3 × 1 grid was used for undoped systems and reduced with respect to the supercell size for doped systems. The atomic positions including the interlayer distances of undoped systems were optimized, and we neglected atomic relaxations in the presence of dopants because they are negligible .

Conflicts of interest

The authors declare no conflict of interest.

Acknowledgment

This work was supported by the Samsung Research Funding Centre of Samsung Electronics (Project Number: SRFC-MA1402-13). The DFT calculations were carried out at the KISTI supercomputing center (KSC-2018-CHA-0038). J.Y.L. acknowledges the support from KU-KIST School project.

Appendix A. Supplementary data

Supplementary data to this article can be found online at https://doi.org/10.1016/j.nanoen.2019.104053.

References

[1] M.G. Walter, E.L. Warren, J.R. McKone, S.W. Boettcher, Q. Mi, E.A. Santori, N.S. Lewis, Chem. Rev. 110 (2010) 6446–6473.
[2] F. Bonaccorso, L. Colombo, G. Yu, M. Stoller, V. Tozzini, A.C. Ferrari, R.S. Ruoff, V. Pellegrini, Science 347 (2015) 1246501.
[3] D. Deng, K. Novoselov, Q. Fu, N. Zheng, Z. Tian, X. Bao, Nat. Nanotechnol. 11 (2016) 218–230.
[4] D. Voiry, H.S. Shin, K.P. Loh, M. Chhowalla, Nat. Rev. Chem. 2 (2018) 0105.
[5] H. Wang, L. Zhang, Z. Chen, J. Hu, S. Li, Z. Wang, J. Liu, X. Wang, Chem. Soc. Rev. 43 (2014) 5234–5244.
[6] S.J.A. Moniz, S.A. Shevlin, D.J. Martin, Z.-X. Guo, J. Tang, Energy Environ. Sci. 8 (2015) 731–759.
[7] S. Zhao, Y. Wang, J. Dong, C.-T. He, H. Yin, P. An, K. Zhao, X. Zhang, C. Gao, L. Zhang, Nat. Energy 1 (2016) 16184.
[8] S. Zhao, D.W. Wang, R. Amal, L. Dai, Adv. Mater. 31 (2019) 1801526.
[9] B. Hinnemann, P.G. Moses, J. Bonde, K.P. Jørgensen, J.H. Nielsen, S. Horch, I. Chorkendorff, J.K. Nørskov, J. Am. Chem. Soc. 127 (2005) 5308–5309.
[10] Y. Li, H. Wang, L. Xie, Y. Liang, G. Hong, H. Dai, J. Am. Chem. Soc. 133 (2011) 7296–7299.
[11] T.F. Jaramillo, K.P. Jørgensen, J. Bonde, J.H. Nielsen, S. Horch, I. Chorkendorff, Science 317 (2007) 100–102.
[12] D. Voiry, H. Yamaguchi, J. Li, R. Silva, D.C.B. Alves, T. Fujita, M. Chen, T. Asefa, V.B. Shenoy, G. Eda, M. Chhowalla, Nat. Mater. 12 (2013) 850–855.
[13] M. Chhowalla, H.S. Shin, G. Eda, L.-J. Li, K.P. Loh, H. Zhang, Nat. Chem. 5 (2013) 263–275.
[14] M.A. Lukowski, A.S. Daniel, F. Meng, A. Forticaux, L. Li, S. Jin, J. Am. Chem. Soc. 135 (2013) 10274–10277.
[15] X. Yu, M.S. Prévot, N. Guijarro, K. Sivula, Nat. Commun. 6 (2015) 7596.
[16] K.C. Kwon, S. Choi, K. Hong, C.W. Moon, Y.-S. Shim, D.H. Kim, T. Kim, W. Sohn, J.-M. Jeon, C.-H. Lee, K.T. Nam, S. Han, S.Y. Kim, H.W. Jang, Energy Environ. Sci. 9 (2016) 2240–2248.
[17] C. Bae, T.A. Ho, H. Kim, S. Lee, S. Lim, M. Kim, H. Yoo, J.M. Montero-Moreno, J.H. Park, H. Shin, Sci. Adv. 3 (2017) e1602215.
[18] D. Voiry, J. Yang, M. Chhowalla, Adv. Mater. 28 (2016) 6197–6206.
[19] Y. Wan, Z. Zhang, X. Xu, Z. Zhang, P. Li, X. Fang, K. Zhang, K. Yuan, K. Liu, G. Ran, Nano Energy 51 (2018) 786–792.
[20] J. Kibsgaard, Z. Chen, B.N. Reinecke, T.F. Jaramillo, Nat. Mater. 11 (2012) 963–969.
[21] D. Kong, H. Wang, J.J. Cha, M. Pasta, K.J. Koski, J. Yao, Y. Cui, Nano Lett. 13 (2013) 1341–1347.
[22] Q. Ding, F. Meng, C.R. English, M. Cabán-Acevedo, M.J. Shearer, D. Liang, A.S. Daniel, R.J. Hamers, S. Jin, J. Am. Chem. Soc. 136 (2014) 8504–8507.
[23] G. Li, D. Zhang, Q. Qiao, Y. Yu, D. Peterson, A. Zafar, R. Kumar, S. Curtarolo, F. Hunte, S. Shannon, Y. Zhu, W. Yang, L. Cao, J. Am. Chem. Soc. 138 (2016) 16632–16638.
[24] J. Deng, H. Li, J. Xiao, Y. Tu, D. Deng, H. Yang, H. Tian, J. Li, P. Ren, X. Bao, Energy Environ. Sci. 8 (2015) 1594–1601.
[25] C. Tsai, H. Li, S. Park, J. Park, H.S. Han, J.K. Nørskov, X. Zheng, F. Abild-Pedersen, Nat. Commun. 8 (2017) 15113.
[26] J. Kang, S. Tongay, J. Zhou, J. Li, J. Wu, Appl. Phys. Lett. 102 (2013) 012111.
[27] C.-H. Lee, G.-H. Lee, A.M. Van Der Zande, W. Chen, Y. Li, M. Han, X. Cui, G. Arefe, C. Nuckolls, T.F. Heinz, J. Guo, J. Hone, P. Kim, Nat. Nanotechnol. 9 (2014) 676–681.
[28] X. Hong, J. Kim, S.-F. Shi, Y. Zhang, C. Jin, Y. Sun, S. Tongay, J. Wu, Y. Zhang, F. Wang, Nat. Nanotechnol. 9 (2014) 682–686.
[29] J. Shi, R. Tong, X. Zhou, Y. Gong, Z. Zhang, Q. Ji, Y. Zhang, Q. Fang, L. Gu, X. Wang, Z. Liu, Y. Zhang, Adv. Mater. 28 (2016) 10664–10672.
[30] X. Cui, G.-H. Lee, Y.D. Kim, G. Arefe, P.Y. Huang, C.-H. Lee, D.A. Chenet, X. Zhang, L. Wang, F. Ye, F. Pizzocchero, B. Jessen, K. Watanabe, T. Taniguchi, D.A. Muller, T. Low, P. Kim, J. Hone, Nat. Nanotechnol. 10 (2015) 534–540.
[31] C.R. Dean, A.F. Young, I. Meric, C. Lee, L. Wang, S. Sorgenfrei, K. Watanabe, T. Taniguchi, P. Kim, K.L. Shepard, J. Hone, Nat. Nanotechnol. 5 (2010) 722–726.
[32] S. Boandoh, S.H. Choi, J.H. Park, S.Y. Park, S. Bang, M.S. Jeong, J.S. Lee, H.J. Kim, W. Yang, J.Y. Choi, S.M. Kim, K.K. Kim, Small 13 (2017) 1701306.
[33] X. Zhang, Q.-H. Tan, J.-B. Wu, W. Shi, P.-H. Tan, Nanoscale 8 (2016) 6435–6450.
[34] S. Kim, K. Kim, J.-U. Lee, H. Cheong, 2D Mater. 4 (2017) 045002.
[35] Y. Yu, S.-Y. Huang, Y. Li, S.N. Steinmann, W. Yang, L. Cao, Nano Lett. 14 (2014) 553–558.
[36] H. Li, C. Tsai, A.L. Koh, L. Cai, A.W. Contryman, A.H. Fragapane, J. Zhao, H.S. Han, H.C. Manoharan, F. Abild-Pedersen, J.K. Nørskov, X. Zheng, Nat. Mater. 15 (2016) 48–53.
[37] Y. Su, C. Liu, S. Brittman, J. Tang, A. Fu, N. Kornienko, Q. Kong, P. Yang, Nat. Nanotechnol. 11 (2016) 609–612.
[38] D. Voiry, R. Fullon, J. Yang, C.d.C.C. e Silva, R. Kappera, I. Bozkurt, D. Kaplan, M.J. Lagos, P.E. Batson, G. Gupta, A.D. Mohite, L. Dong, D. Er, V.B. Shenoy, T. Asefa, M. Chhowalla, Nat. Mater. 15 (2016) 1003–1009.
[39] J.M. Velazquez, J. John, D.V. Esposito, A. Pieterick, R. Pala, G. Sun, X. Zhou, Z. Huang, S. Ardo, M.P. Soriaga, B.S. Brunschwig, N.S. Lewis, Energy Environ. Sci. 9 (2016) 164–175.
[40] H. Li, M. Du, M.J. Mleczko, A.L. Koh, Y. Nishi, E. Pop, A.J. Bard, X. Zheng, J. Am. Chem. Soc. 138 (2016) 5123–5129.
[41] J. Zhang, J. Wu, H. Guo, W. Chen, J. Yuan, U. Martinez, G. Gupta, A. Mohite, P.M. Ajayan, J. Lou, Adv. Mater. 29 (2017) 1701955.
[42] R.S. Hutton, D.E. Williams, Anal. Chem. 67 (1995) 280–282.
[43] K.Y. Kim, J. Lee, S. Kang, Y.-W. Son, H.W. Jang, Y. Kang, S. Han, ACS Catal. 8 (2018) 4508–4515.
[44] Y. Kang, S. Han, Nanoscale 9 (2017) 4265–4271.
[45] G. Kresse, J. Furthmüller, Phys. Rev. B 54 (1996) 11169–11186.
[46] J.P. Perdew, K. Burke, M. Ernzerhof, Phys. Rev. Lett. 77 (1996) 3865–3868.
[47] S. Grimme, J. Antony, S. Ehrlich, H. Krieg, J. Chem. Phys. 132 (2010) 154104.

Jae Yoon Lee received his B.S. from Kyunghee University in 2015. He is currently a Ph.D. candidate under the supervision of Prof. Chul-Ho Lee at KU-KIST graduate School of Converging Science and Technology, Korea University, Korea. His current research interests focus on the low dimensional materials and its (photo)electrochemical energy application such as catalysis, energy storage and conversion.

Sungwoo Kang received a B.S. from Seoul National University in 2016. He is currently a Ph.D. candidate under the guidance of Prof. Seungwu Han at Department of Materials Science and Engineering in Seoul National University. His research focuses on the first-principles investigations of low dimensional materials for the electrochemical catalysis and light-emitting devices.

Dr. Donghun Lee is a research professor in the KU-KIST Graduate School of Converging Science and Technology at Korea University, Korea. He received Ph.D. and B.S. degrees in material science and engineering from Pohang University of Science and Technology (POSTECH), Korea. His research interests include electronics and photonics based on low dimensional materials.

Dr. Ki Chang Kwon is a postdoctoral research fellow under the supervision of Prof. Ho Won Jang at Department of Materials Science and Engineering, Seoul National University. His research focuses on the synthesis of various 2-dimensional materials via chemical vapor deposition and its applications to optoelectronic devices.

Dr. Seokhoon Choi is a postdoctoral research fellow under the supervision of Prof. Ho Won Jang at Department of Materials Science and Engineering, Seoul National University. His research focuses on the synthesis of various 2-dimensional materials via chemical vapor deposition and its applications to (photo)electrochemical water splitting.

Soo Ho Choi received his B.S. degree in 2015. Now he is pursuing Ph.D. degree in the department of physics at Dongguk University. He is studying the growth and growth mechanism of transition metal dichalcogenides by means of chemical vapor deposition.

Seunghoon Yang received his B.S. from Korea University in 2016. He is currently a Ph.D. candidate under the supervision of Prof. Chul-Ho Lee at KU-KIST graduate School of Converging Science and Technology, Korea University, Korea. His current research interests focus on optoelectronics based on 2D materials.

Dr. Soo Min Kim is currently a Senior Researcher in Korea Institute of Science and Technology, Republic of Korea. She received her M.S and Ph.D. degrees in SKKU Advanced Institute of Nano Technology from Sungkyunkwan University in 2008 and 2011. She was a postdoctoral fellow at Massachusetts Institute of Technology (MIT) from 2011 to 2012. Her research interests focus on synthesis of wafer-scale single-crystal 2D materials including graphene, hexagonal boron nitride and transition metal dichalcogenides and their applications in gas barrier and hydrogen evolution reaction for hydrogen production.

Kangwon Kim is a Ph.D. candidate under the supervisor, Prof. Hyeonsik Cheong, in the Department of Physics at Sogang University, where he received his B.S. and M.S. degrees in 2014 and 2016, respectively. His research focuses on the physical properties of 2-dimensional materials by using optical spectroscopy.

Jihoon Kim received his B.S. from the Department of Materials Science and Chemical Engineering at Hanyang University in 2017. He is currently a Ph.D candidate under the supervision of Prof. Jungwon Park at the Department of Chemical and Biological Engineering at Seoul National University. His research area includes the synthesis and chemical reactions of 2D transition metal chalcogenides and characterization of low-dimensional materials.

Yoonseok Kim received his B.S. from Yonsei University in 2017. He is currently a Ph.D. candidate at KU-KIST graduate School of Converging Science and Technology, Korea University, Korea. His current research interests focus on optoelectronics device using the low dimensional vdW materials

Prof. Jungwon Park received B.S. from the Department of Chemistry at Pohang University of Science and Technology, South Korea. He received his Ph.D from the Department of Chemistry at University of California, Berkeley in 2012. After that, he performed his postdoc research in the School of Engineering and Applied Sciences at Harvard University from 2012 to 2016. He is currently an assistant professor in the School of Chemical and Biological Engineering at Seoul National University, South Korea. He is jointly affiliated to the Center for Nanoparticle Research, Institute for Basic Science. His research interests include physical chemistry of solid materials, in-situ liquid-phase TEM, interface chemistry, and synthesis of low-dimensional materials.

Haeli Park received his M.S. from KU-KIST graduate School of Converging Science and Technology, Korea University, Korea in 2018. She is currently working at Samsung Electronics.

Woong Huh received his B.S. from Korea University in 2016. He is currently a Ph.D. candidate under the supervision of Prof. Chul-Ho Lee at KU-KIST graduate School of Converging Science and Technology, Korea University, Korea. His current research interests focus on data storage devices and their neuromorphic applications using the two-dimensional vdW materials and analysis for low-power design.

Hee Seong Kang received his B.S. degree from Sejong University in 2014. He is currently a Ph.D. candidate under the supervision of Prof. Chul-Ho Lee at KU-KIST graduate School of Converging Science and Technology, Korea University, Korea. His current research interests focus on the two-dimensional semiconductors growth and engineering for practical applications.

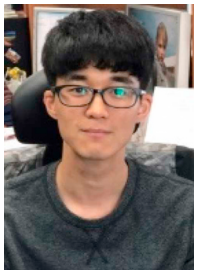

Seong Won Lee received his B.S. degree in physics from Korea University, Seoul, Korea, in 2017. He is currently a Ph.D. candidate under the supervision of Prof. Hong-Gyu Park at Korea University. His current research interests include demonstration of single photon emitters coupled to waveguides.

Prof. Hong-Gyu Park received B.S., M.S., and Ph.D. degrees in physics from Korea Advanced Institute of Science and Technology, Daejeon, Korea, in 1998, 2000, and 2004, respectively. He was a post-doctoral fellow with the Department of Chemistry, Harvard University, Cambridge, MA, from 2005 to 2007. In 2007, he joined the Department of Physics, Korea University, Seoul, Korea, where he is currently a full professor. His current research interests include sub wavelength plasmonic laser/cavity structures, nanoscale photovoltaic devices, nanowire transistors/photodetectors, and neural recording using nanostructures.

Prof. Min Jae Ko is a full professor in the Department of Chemical Engineering at Hanyang University, Korea. He received Ph.D degrees at Seoul National University in 2001. After that, he performed his postdoc research at Massachusetts Institute of Technology, from 2001 to 2004. Then he joined Samsung Electronics Co., as a senior research engineer in 2005. From 2008 to 2017, he worked for the Photo-Electronic Hybrids Research Center at KIST. His research focuses on the advanced materials, devices, and processing for the next generation energy harvesting devices. Prof. Ko has published over 150 papers in peer-reviewed journals, and 50 registered patents.

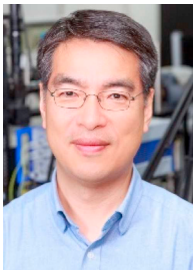

Prof. Hyeonsik Cheong is a professor of physics at Sogang University in Seoul, Korea. He received his B.S. degree in physics from Seoul National University and A.M. and Ph.D. in physics from Harvard University. After working at Harvard as a postdoctoral fellow and at National Renewable Energy Laboratory, he joined the Department of Physics at Sogang University in 1999. His research interest includes spectroscopic studies of graphene and 2-dimensional materials, semiconductor nanostructures, and solar cell materials. He is currently serving as the Chair of the Division of Applied Physics of the Korean Physical Society.

Prof. Seungwu Han is a professor in Department of Materials Science and Engineering, Seoul National University. He completed a Ph.D. in Physics at Seoul National University in 2000. His research interests are first-principles studies and data-driven researches of functional materials and low dimensional materials in the application of high-k dielectrics, *p*-type transparent conducting oxides, phase-change memories, light-emitting devices, and electrochemical catalysis.

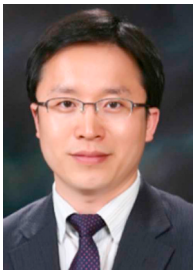

Prof. Ho Won Jang is an associate professor in Department of Materials Science and Engineering, Seoul National University. He received his Ph.D. from the Department of Materials Science and Engineering of Pohang University of Science and Technology in 2004. His research interests include the synthesis of metal oxide thin films, 2-dimensional materials, and halide perovskites, and the application of those materials to various devices including chemical sensors for electronic nose and tongue, photoelectrochemical water splitting cells, memristors, optoelectronics, smart windows, and nanophotonics.

Prof. Chul-Ho Lee received his B.S. (2005) and Ph.D. (2011) from the Department of Materials Science and Engineering of Pohoang University of Science and Technology (POSTECH), Korea. After his Ph. D course, he worked in the Department of Physics at Columbia University, United States, as a postdoctoral fellow. In 2014, then, he joined the faculty of the KU-KIST Graduate School of Converging Science and Technology at Korea University. His current researches focus on the growth, characterization and applications of low-dimensional nanomaterials such as 2D semiconductors and graphene.